

RESEARCH

Open Access



# Mechanical Characteristics of Hybrid-Fiber-Reinforced Concrete Shaft Wall Structure Under Uneven Load

Zhishu Yao<sup>\*</sup> , Yongjie Xu, Ping Zhang, Yu Fang, Chen Wang, Naihao Diao and Kun Hu

## Abstract

To prevent damage to shaft walls in mines due to uneven loading, the mechanical properties of a shaft wall structure made of hybrid-fiber-reinforced concrete were studied. First, through orthogonal testing, the optimal mix proportion of the hybrid-fiber-reinforced concrete was obtained. Subsequently, a numerical calculation model of the shaft wall structure under uneven loading was established. The calculation results showed that the structure exhibits a tensile stress under the action of uneven loading and that its bearing capacity can be improved using the hybrid-fiber-reinforced concrete. Based on the numerical simulation results, a calculation formula for the bearing capacity of the shaft wall was obtained by regression. Finally, a model test was conducted on the shaft lining structure. The results obtained were consistent with those obtained using the numerical simulation regression formula, confirming the reliability of the numerical simulation results. This study showed that a hybrid-fiber-reinforced concrete shaft wall structure can better withstand uneven loads and has improved brittle failure characteristics. Hybrid-fiber-reinforced concrete is an excellent material for deep shaft wall structures.

**Keywords:** uneven load, mine shaft wall, hybrid fibers, concrete, mechanical properties

## 1 Introduction

The exploitation of deep mineral resources requires the construction of vertical shafts as channels for personnel movement, ventilation, drainage, and ore lifting (He, 2021; Liu et al., 2021). The supporting structure of such shafts is called the shaft wall structure (Cui, 2003). Based on geological exploration data, a wellbore typically passes through complex formations, such as loose layers, bedrock weathering zones, stable bedrock, bedrock fracture zones, and coal seams, from the ground to the mining level. Therefore, the stress conditions in the shaft wall become complex during the development of deep mines. For example, in deep rock formations, due

to the difference in the lithology, rock formation inclination, fracture zone, faults, and structural stress, a shaft is subjected to an uneven load in the horizontal direction, which worsens the force conditions of the shaft and easily inflicts damage to the shaft wall structure (Gao et al., 2021; Zhang et al., 2014). Moreover, the rock cover movement caused by mining produces an uneven load effect on close-range shafts, causing the shaft to be deflected and damaged, which seriously threatens the safe operation of the shaft (Cheng et al., 2021).

When a newly established wellbore drilled using the manual refrigeration method requires crossing a deep and loose layer, the outer wall is mainly subjected to the force from the frozen wall, which is called the freezing pressure (Jiang et al., 2013; Yao et al., 2015). However, in an actual project, due to the deflection of the freezing hole and the uneven distribution of the brine flow, the freezing pressure of the outer wall exhibits uneven characteristics (Shu et al., 2021; Zhang et al., 2018).

Journal information: ISSN 1976-0485 / eISSN 2234-1315

\*Correspondence: zsyao@aust.edu.cn

School of Civil Engineering and Architecture, Anhui University of Science and Technology, Huainan 232001, China



© The Author(s) 2022. **Open Access** This article is licensed under a Creative Commons Attribution 4.0 International License, which permits use, sharing, adaptation, distribution and reproduction in any medium or format, as long as you give appropriate credit to the original author(s) and the source, provide a link to the Creative Commons licence, and indicate if changes were made. The images or other third party material in this article are included in the article's Creative Commons licence, unless indicated otherwise in a credit line to the material. If material is not included in the article's Creative Commons licence and your intended use is not permitted by statutory regulation or exceeds the permitted use, you will need to obtain permission directly from the copyright holder. To view a copy of this licence, visit <http://creativecommons.org/licenses/by/4.0/>.

This adversely affects the stress acting on the shaft wall, because of which the external wall is stretched and damaged. For example, in the return air shaft in the East of Guqiao Mining Group, when the shaft wall was excavated to a depth of 300 m, the outer wall of the upper range of nearly 10 m was ruptured. From the destruction form and the actual measured freezing pressure of the shaft wall, the freezing pressure on the outer wall was found to be evidently uneven, which was the main reason for the failure of the shaft wall at this location (Yang & Li, 2016). In another example, when the side wall of Gubei Coal Mine was excavated and after shaft construction, the outer wall was seriously damaged, and an analysis showed that the uneven freezing pressure was the main reason for the tensile damage of the concrete of the shaft wall (Zhao & Lin, 2014).

To prevent tensile damage of the concrete, the tensile performance of shaft walls should be improved (Liang et al., 2021). In recent years, scholars have put forward constructive suggestions for improving the shaft wall structure. For example, Wang and Qi (2005) outlined two feasible methods to improve the bearing capacity of a shaft lining structure on the premise of ensuring a reasonable shaft lining thickness: one is to use steel or steel plate concrete composite shaft lining and increase the steel content in the structure; although this method can improve its strength, it significantly increases the construction cost of shaft lining. The second method is to improve the strength grade of concrete (i.e., using concrete materials with high strength and high toughness). The latter method is more economical and feasible, thus widely used in China.

Due to the strong brittleness of high-strength concrete, fiber is typically added to improve the tensile strength of members in structural applications (Fang et al., 2022; Guler & Yavuz, 2019; Guler et al., 2019a). For example, to prevent the excessive formation of cracks and serious water leakage due to the temperature stress in a shaft wall, Yang et al. (2019) prepared excellent building materials for concrete walls by adding mixed fibers and expanding agents, and conducted anti-seepage, anti-cracking, and microscopic tests. The cracking and water seepage problems of the shaft wall could be resolved. Shi et al. (2020) studied the mechanical properties of basalt polypropylene fiber-mixed reinforced concrete under different compressive strengths through experiments. The experiments proved that polypropylene fiber can improve the flexural strength by approximately 20%. Hsieh et al. (2008) mixed two types of polypropylene fibers with different sizes into concrete. The test results showed that the compressive strength, splitting tensile strength, and bending resistance of polypropylene hybrid-fiber high-strength concrete were better than those of single-fiber

high-strength concrete. Guler et al. (2019b) proposed a new strength prediction model to predict the compressive, tensile, and flexural strengths of hybrid-fiber high-strength concrete in view of the drawbacks of the concrete strength prediction model.

The above summarizes the research progress on hybrid-fiber concrete in terms of toughness enhancement. In terms of numerical calculation of the shaft lining structure, Han et al. (2012) employed the ANSYS finite element software to simulate the horizontal bearing characteristics of a composite steel fiber-mixed high-strength concrete shaft lining, obtained the factors influencing the horizontal ultimate bearing capacity through numerical simulation, and derived a calculation formula for the horizontal ultimate bearing capacity. Based on the principle and method of fuzzy random finite element, Yao et al. (2016) employed ANSYS to numerically calculate the fuzzy random finite element reliability of an outer shaft lining structure. The results showed that the obtained reliability can better reflect the actual working conditions.

Qin et al. (2017) studied the compressive strength and failure characteristics of hybrid-fiber-reinforced concrete shaft in a mine shaft wall through a uniform loading test. The results showed that the hybrid-fiber-reinforced concrete shaft wall had a slightly higher compressive strength than the shaft wall structure made of ordinary high-strength concrete and had better plasticity and deformation resistance. Yao et al. (2019) prepared a hybrid-fiber-reinforced concrete structure model and applied a uniform load through a hydraulic loading device; the hybrid-fiber-reinforced concrete shaft wall structure exhibited an evident plastic flow deformation stage during the loading process, which could improve the brittleness failure characteristics of the shaft wall.

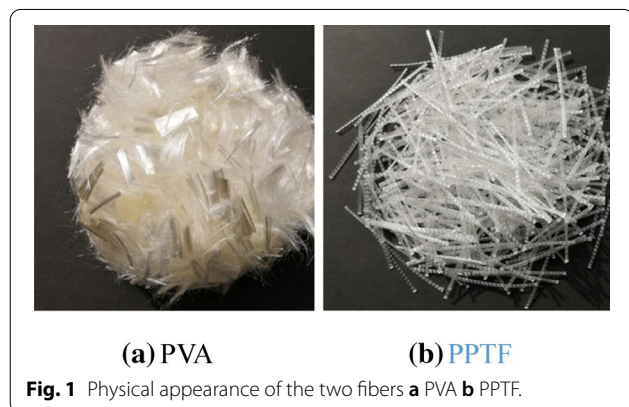
Current research on hybrid-fiber-reinforced concrete shaft walls has mainly focused on their material preparation and basic mechanical properties; only uniform loading has been applied in the model tests on shaft wall structures, which is inconsistent with the force condition of such structures observed in actual construction through deep formations. Hence, to analyze the actual force state of the outer wall of the vertical shaft in deep rock formations and frozen shafts in deep loose layers and to evaluate the reliability of the shaft wall, it is important to study the mechanical characteristics of the vertical shaft wall under uneven loading.

## 2 Preparation of Hybrid-Fiber-Reinforced Concrete for Vertical Shaft Wall

Based on the requirements of safe and efficient construction of vertical shaft walls for mines, this test adopts raw materials commonly used in engineering sites to prepare

**Table 1** Basic performance indices of fiber.

Fiber type	Length/mm	Diameter/ $\mu\text{m}$	Initial modulus/GPa	Elongation/%	Density/ $\text{g cm}^{-3}$	Tensile strength/MPa
PPTF	50	1200 $\pm$ 200	5	24	0.91	570
PVA	18	15 $\pm$ 3	39	6.9	1.30	1830



hybrid-fiber-reinforced concrete for the shaft wall (Kong et al., 2020; Yao et al., 2009). P. O 52.5R ordinary Portland early strength cement was selected as the basic cementitious material. A coarse aggregate was selected as the continuous graded basalt gravel with a particle size range of 5–20 mm, and its crushing index was 6.7%. Natural river sand was selected as the fine aggregate with a fineness modulus of 2.934 and a mud content less than 1.6%. NF-F concrete composite was selected as the admixture, and its main components were fly ash, fine grinding slag, silica fume, and high range water reducer.

The fiber materials were polyvinyl alcohol fiber (PVA) and polypropylene imitation steel fiber (PPTF). Polypropylene-imitated steel fiber is a substitute made based on the advantages of steel fibers, while having some advantages of synthetic fibers. Compared with steel fibers, it has the characteristics of corrosion resistance, easy dispersion, easy construction, and no damage to mixing equipment. Table 1 presents the basic performance indices (Yao et al., 2021). Fig. 1 shows the physical appearance.

In this preparation test of the hybrid-fiber-reinforced concrete, based on the commonly used mixture ratios of C60, C70, and C80 in engineering (China Coal Construction Association, 2016; Sun & Yao, 2017), a test was conducted by adding different contents of hybrid fibers. Therefore, an orthogonal test was conducted on three factors, namely the concrete strength grade, polyvinyl alcohol fiber (PVA) volume content, and polypropylene-imitated steel fiber (PPTF) volume content, with three

**Table 2** Orthogonal test design.

Specimen	Concrete strength grade/MPa	PVA volume content/%	PPTF volume content/%
H-1	C60	0.056	0.440
H-2	C60	0.084	0.549
H-3	C60	0.112	0.659
H-4	C70	0.056	0.659
H-5	C70	0.084	0.549
H-6	C70	0.112	0.440
H-7	C80	0.056	0.549
H-8	C80	0.084	0.440
H-9	C80	0.112	0.659

levels set for each factor. In this experiment, the concrete strength levels were separately set to C60, C70, and C80; the volume content levels of the polyvinyl alcohol fiber were set to 0.056%, 0.084%, and 0.112%; the volume contents of the polypropylene-imitated steel fiber were set to 0.440%, 0.549%, and 0.659%, respectively. Based on the orthogonal test method, nine groups of experiments were required, as shown in Table 2.

Through orthogonal test and a large number of repetitive tests, the mix proportion of the hybrid-fiber-reinforced concrete for the shaft wall was obtained, as shown in Table 3.

### 3 Numerical Simulation of the Shaft Wall Structure Under Uneven Load

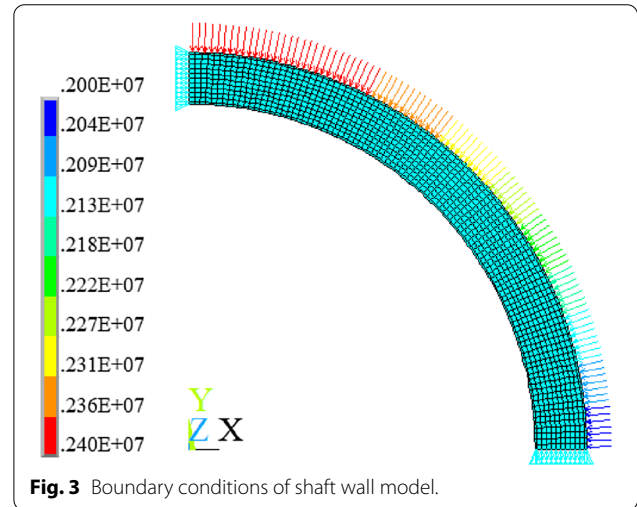
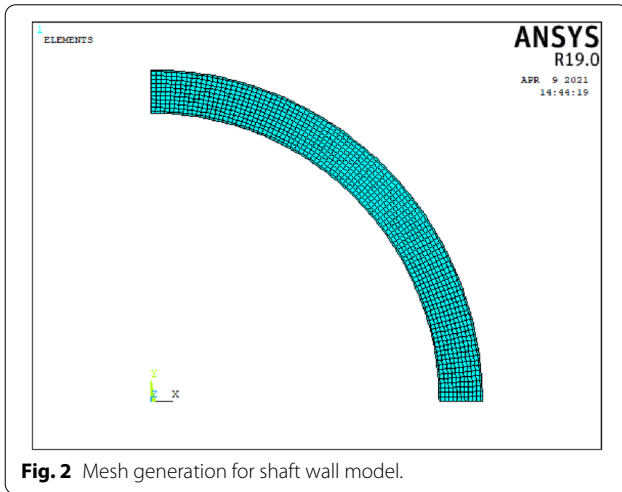
#### 3.1 Establishment of the Calculation Model

##### 3.1.1 Element Type

Using ANSYS, a finite element model of the hybrid-fiber-reinforced concrete shaft wall structure was established. Short-section excavation construction is typically adopted for the shaft wall of vertical shafts in deep rock strata and for the outer wall of frozen shafts in deep loose layers, and the height of the construction section is typically in the range of 2.0–4.0 m, resulting in many ballast joints and discontinuities in the vertical direction of the shaft wall. Therefore, the shaft wall structure can be considered a case of plane stress problem, that is, a plane stress model was adopted for the numerical calculation. The four-node 2D solid plane 182 element was selected as the concrete element, which has the characteristics of

**Table 3** Mix ratio of hybrid-fiber-reinforced concrete.

Strength grade	Water-to-binder ratio	Cement/ kg m <sup>-3</sup>	Admixture/ kg m <sup>-3</sup>	Basalt gravel/ kg m <sup>-3</sup>	Percentage of sand/%	PVA content/ %	PPTF content/ %
HFRC 60	0.28	410	130	1121.5	36	0.084	0.549
HFRC 70	0.27	420	140	1111.0	36	0.084	0.549
HFRC 80	0.26	430	155	1096.3	36	0.084	0.549



stress stiffness, hyperelasticity, large deformation, and high strain, and can simulate the deformation of incompressible hyperelastic materials; link180 element was selected as the reinforcement; in this element, each node has three degrees of freedom and is translational along the three directions of the node. Owing to the symmetrical structure and symmetrical load, 1/4 of the shaft wall structure was used for the simulation. During grid division, the displacement coordination between the reinforcement and concrete can be realized through joint sharing, as shown in Fig. 2.

**3.1.2 Boundary Condition**

Circumferential displacement constraints are imposed on the two end faces of the wellbore model to allow radial displacement of the wellbore. As for the form of the uneven load distribution, this numerical simulation adopts the sinusoidal expression specified in China’s code for design of coal mine shafts and chambers (China Coal Construction Association, 2016), that is:

$$P = P_0(1 + \beta \sin \theta). \tag{1}$$

Here,  $P$  is the uneven load;  $P_0$  is the minimum load;  $\beta$  is the coefficient of the uneven load;  $\theta$  is the angle between the calculated section and the minimum load.

Fig. 3 shows the boundary conditions of the model.

**3.1.3 Boundary Condition**

Fiber is used to improve the flexural tensile properties of concrete by taking advantage of its high tensile strength and high elongation. In the simulation calculation, to reflect the performance of hybrid fibers, a multilinear follow-up strengthening constitutive model is adopted for the hybrid-fiber-reinforced concrete, and the William and Warnke five-parameter criterion is adopted as the failure criterion (Naser & Hawileh, 2018). The values of the uniaxial tensile strength and compressive strength parameters were derived from basic tests. Table 4 lists its parameters; the ideal elastic–plastic constitutive model is adopted for the reinforcement.

**3.2 Calculation Scheme of the Numerical Simulation**

Based on the theoretical analysis of the shaft wall structure design, the main factors affecting the strength and deformation of the shaft wall structure under uneven loading include the thickness-to-diameter ratio of the shaft wall ( $\lambda$ ) (mean ratio of the shaft wall thickness to the internal diameter), nonuniform load coefficient ( $\beta$ ), and strength grade of the hybrid-fiber-reinforced concrete (HFRC). Therefore, the three factors here were

selected for a comprehensive analysis, with three levels set for each factor. The three-factor and three-level orthogonal simulation scheme was adopted, and a total of nine numerical simulation calculations were required.

To ensure that the research results have universal significance, through the analysis of the design parameters used in mine shaft wall engineering, three shaft wall thicknesses, representative of thin, medium, and thick walls, were selected for the calculation, defined as dimensionless, namely the thickness-to-diameter ratio

( $\lambda$ ). The inner radius of the shaft wall was 5.0 m, the thicknesses of the shaft wall were 0.5, 0.75, and 1.0 m, respectively, and the corresponding thickness-to-diameter ratios were 0.1, 0.15, and 0.2, respectively. Table 5 presents the specific orthogonal simulation design table.

The parameters of the hybrid-fiber-reinforced concrete were named HFRC60, HFRC70, and HFRC80, referring to literature (Zhang et al., 2020); Table 6 presents the specific values. The elastic modulus and

**Table 4** William and Warnke failure criterion parameters for concrete.

Serial number	Parameter	Meaning	Value range
1	ShrCf-Op	Shear transfer coefficient of crack opening (i.e., cracking)	0–1
2	ShrCf-CI	Shear transfer coefficient of crack closure (i.e., crushing)	0–1
3	UnTensSt	Uniaxial tensile strength	Value taken according to test results
4	UnComSt	Uniaxial compressive strength	Value taken according to test results
5	BiComSt	Biaxial compressive strength	$1.2F_C$ , where $F_C$ is the uniaxial compressive strength

**Table 5** Orthogonal design table for numerical simulation.

Model number	Thickness-to-diameter ratio	Design strength of hybrid-fiber-reinforced concrete	Nonuniform pressure coefficient
M-1	0.1	HFRC60	0.1
M-2	0.1	HFRC70	0.2
M-3	0.1	HFRC80	0.3
M-4	0.15	HFRC60	0.2
M-5	0.15	HFRC70	0.3
M-6	0.15	HFRC80	0.1
M-7	0.2	HFRC60	0.3
M-8	0.2	HFRC70	0.2
M-9	0.2	HFRC80	0.1

**Table 6** Mechanical parameters of the shaft wall made of hybrid fiber concrete.

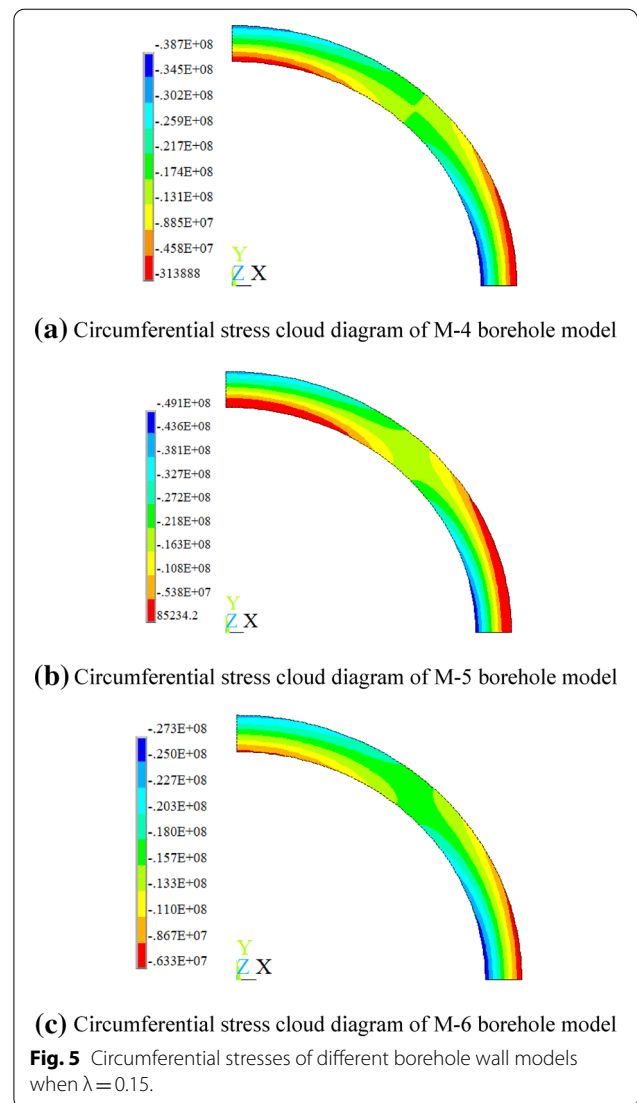
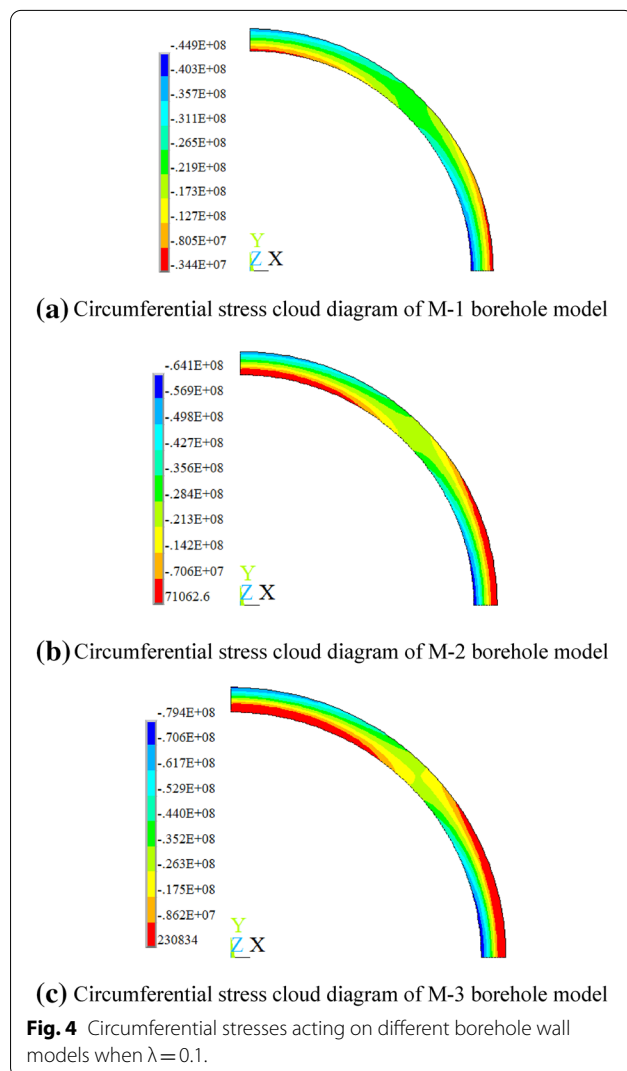
Model number	HFRC	Compressive strength/MPa	Yield stress/MPa	Peak strain/ $\mu\epsilon$	Elastic modulus/MPa	Poisson's ratio
M-1	HFRC60	74.5	62.19	$2.236 \times 10^{-3}$	$3.741 \times 10^4$	0.216
M-2	HFRC70	81.0	68.45	$2.261 \times 10^{-3}$	$3.825 \times 10^4$	0.210
M-3	HFRC80	92.4	73.29	$2.287 \times 10^{-3}$	$3.873 \times 10^4$	0.206
M-4	HFRC60	74.5	62.19	$2.236 \times 10^{-3}$	$3.741 \times 10^4$	0.216
M-5	HFRC70	81.0	68.45	$2.261 \times 10^{-3}$	$3.825 \times 10^4$	0.210
M-6	HFRC80	92.4	73.29	$2.287 \times 10^{-3}$	$3.873 \times 10^4$	0.206
M-7	HFRC60	74.5	62.19	$2.236 \times 10^{-3}$	$3.741 \times 10^4$	0.216
M-8	HFRC70	81.0	68.45	$2.261 \times 10^{-3}$	$3.825 \times 10^4$	0.210
M-9	HFRC80	92.4	73.29	$2.287 \times 10^{-3}$	$3.873 \times 10^4$	0.206

Poisson's ratio of the reinforcement are  $2.1 \times 10^5$  MPa and 0.3, respectively; the yield stress is 340 MPa.

### 3.3 Analysis of Numerical Simulation Results

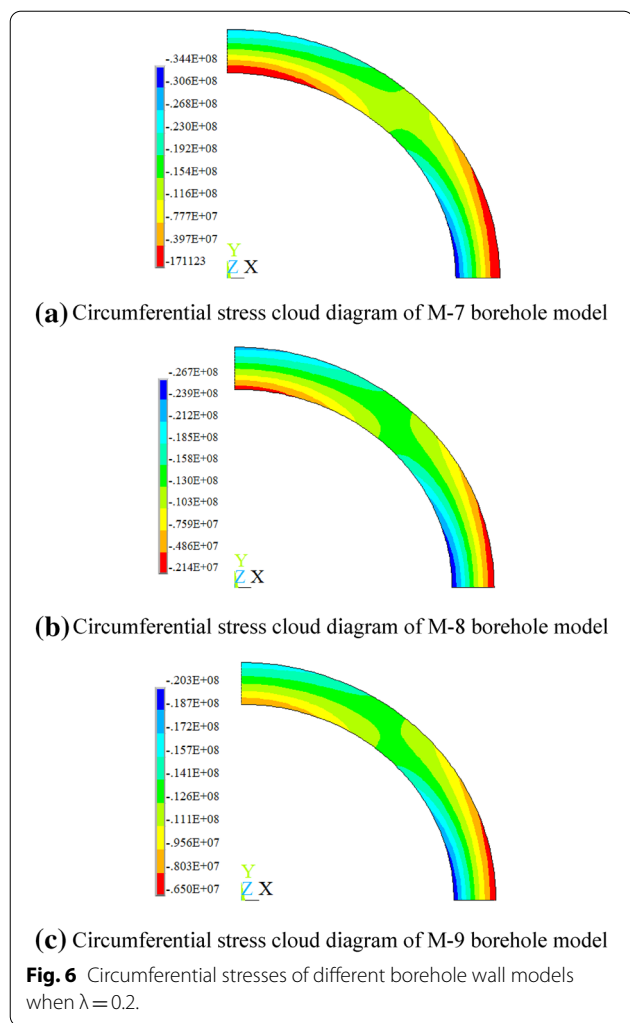
The stress of the hybrid-fiber-reinforced concrete shaft wall under uneven frozen pressures was simulated by applying an uneven load to the hybrid-fiber-reinforced concrete shaft wall structure under different thickness-to-diameter ratios and strength grades. Figs. 4, 5, 6 show the circumferential stress nephograms of each shaft wall model, respectively.

Fig. 4 shows that the circumferential stress distribution of the shaft wall structure also exhibits evident nonuniformity under a nonuniform load. In comparison, the circumferential stress decreases gradually at the inner edge of the shaft wall from  $0^\circ$  to  $90^\circ$  and increases gradually at the outer edge of the shaft wall from  $0^\circ$  to  $90^\circ$ . The circumferential stress is maximum at  $0^\circ$  at the inner edge



and  $90^\circ$  at the outer edge and is minimum at  $90^\circ$  at the inner edge and  $0^\circ$  at the outer edge.

When the thickness-to-diameter ratio is 0.1, by comparing the three diagrams, it can be found that with the increase in the nonuniformity coefficient, the maximum circumferential stresses in the borehole wall and outer edge increase, whereas the minimum circumferential stresses decrease, even under tension. This means that the nonuniform stress distribution is more evident and that the stress acting on the borehole wall is more unfavorable. When the low load is 2 MPa and  $\beta = 0.1$ , the maximum circumferential compressive stress of the M-1 model is 44.9 MPa, and the minimum compressive stress is 3.44 MPa. When the nonuniform load coefficient is 0.2, the maximum circumferential compressive stress of the M-2 model is 64.1 MPa, and the tensile



stress occurs at 90° at the inner edge and 0° at the outer edge of the well wall. Under the action of uneven load, for which the nonuniform load coefficient is 0.3, the maximum compressive stress of the M-3 model reaches 79.4 MPa, and the tensile stress increases at 90° at the inner edge and 0° at the outer edge of the well wall, reaching 0.23 MPa. Because of the poor tensile properties of ordinary concrete, particularly at the early stage of concrete placement, the concrete is vulnerable to tensile damage after the occurrence of tensile stress in the shaft wall. When a hybrid-fiber-reinforced concrete is used, its tensile strength is significantly increased, which significantly improves the resistance of the shaft wall to uneven loads and prevents damage of the shaft wall structure due to uneven loads.

As shown in Fig. 5, with the increase in the thickness-to-diameter ratio, the circumferential stresses in the borehole wall and on the outer edge have the same distribution law as before; however, the value decreases

significantly. Moreover, if the thickness–diameter ratio is 0.15, tension stresses occur only in the direction of the outer edge at 0° and inner edge at 90° under a nonuniformity coefficient of 0.3, while no tension stresses occur under a low nonuniformity coefficient.

As shown in Fig. 6, when the wall thickness-to-diameter ratio is further increased, under three groups of nonuniform loads, the circumferential stresses of the inner and outer edges of the shaft wall are both compressive stresses, and there is no tensile stress. At the same time, the circumferential stress is lower, and there is less influence of the uneven load on the shaft wall. Meanwhile, by observing the M-1 to M-9 stress clouds, it can be found that the circumferential stress is maximum at the inner edge boundary of the low load.

The above simulation calculation results show that under the action of the uneven load, the shaft wall structure exhibits a tensile stress, while the tensile strength of common concrete is low. In particular, in the early stage of concrete construction, its tensile strength is lower, which is unfavorable to the stress condition of the shaft wall structure. Although increasing the shaft wall thickness can effectively resist the action of uneven load, the construction cost will be significantly increased, and the construction process will be more difficult. Therefore, when considering a nonuniform frozen pressure, it is an effective technical way to improve the resistance of the shaft wall to nonuniform loads by using hybrid-fiber-reinforced concrete instead of ordinary concrete as the wall building material to improve the tensile capacity of the material itself.

### 3.4 Analysis of the Ultimate Bearing Capacity of Hybrid-Fiber-Reinforced Concrete Shaft Wall Structure

The ultimate bearing capacity of the shaft wall model (taking a low load  $P_0$ ) was obtained by applying a step-wise load to the calculation model until failure. Table 7 presents the results.

From Table 7, it can be found that the bearing capacity of the shaft wall increases significantly with the increase in the thickness-to-diameter ratio and concrete strength under the uneven load. However, with the increase in the nonuniform pressure coefficient, the bearing capacity of the shaft wall decreases. A further comparison shows that with the increase in the wall thickness, the influence of the nonuniform pressure coefficient is lower.

To analyze the influence of various factors on the bearing capacity of the shaft wall, the calculation results were analyzed by conducting a range analysis; Table 8 presents the results. The concrete strength, wall thickness-to-diameter ratio, and nonuniform pressure coefficient were taken as factors A, B, and C, respectively.

**Table 7** Ultimate bearing capacity of shaft wall structure.

Model number	Thickness-to-diameter ratio/ $\lambda$	Nonuniform pressure coefficient/ $\beta$	Compressive strength of concrete/MPa	Ultimate bearing capacity/MPa
M-1	0.1	0.1	74.5	2.7
M-2	0.1	0.2	81.0	3.3
M-3	0.1	0.3	92.4	4.0
M-4	0.15	0.2	74.5	4.2
M-5	0.15	0.3	81.0	4.9
M-6	0.15	0.1	92.4	6.9
M-7	0.2	0.3	74.5	6.3
M-8	0.2	0.2	81.0	7.6
M-9	0.3	0.1	92.4	10.5

**Table 8** Range analysis results.

Factor level	A	B	C	Factors from major to minor
Ultimate bearing capacity				
K1	4.40	3.33	6.70	BAC
K2	5.27	5.33	5.03	
K3	7.13	8.13	5.07	
R	2.73	4.80	1.67	

By comparing the R value in Table 8, it can be seen that the influence order for the ultimate bearing capacity of the hybrid-fiber-reinforced concrete shaft wall structure is the wall thickness-to-diameter ratio, strength of the hybrid-fiber-reinforced concrete, and nonuniform pressure coefficient.

The objective was to obtain the relationship between the ultimate bearing capacity ( $P_0$ ) of the hybrid-fiber-reinforced concrete shaft wall structure under uneven load and the concrete strength ( $f_{cu}$ ), shaft thickness-to-diameter ratio ( $\lambda$ ), and uneven coefficient ( $\beta$ ). To this end, through dimension analysis method and numerical simulation results, the Origin regression was used to establish the calculation formula for the bearing capacity of the shaft wall under nonuniform loading with a sinusoidal distribution as follows:

$$P_0 = 0.0054 \cdot f_{cu}^{2.1167} \cdot \lambda^{1.321} \cdot \beta^{-0.0513} \quad (2)$$

#### 4 Large-Scale Model Test of Hybrid-Fiber-Reinforced Concrete Shaft Wall Structure

To further study the mechanical characteristics of the hybrid-fiber-reinforced concrete shaft wall structure under uneven load and verify the numerical simulation results, a simulation test was conducted on the large

shaft wall structure using the loading device in the underground engineering section of Anhui University of Science and Technology.

#### 4.1 Model Design of Shaft Wall

##### 4.1.1 Derivation of the Similarity Criterion

In wall engineering, short-section excavation and lining construction is adopted. Similar to the numerical simulation, the model test also adopts the plane stress model.

Due to its large geometry and high bearing capacity, it is challenging to conduct full-scale tests on this type of high-performance shaft wall structure; therefore, a reduced-scale model test was conducted in this study. The common scale model test has size effect, which is quite different from the actual stress conditions, resulting in inaccurate measurement results. To reduce the error caused by the size effect, the similarity criterion is used to guide the model test. Based on the balance equation, geometric equation, and physical equation, the similarity criterion for the model test was established as follows (Yang, 2005):

$$\frac{C_\varepsilon \cdot C_l}{C_u} = 1, \frac{C_{\bar{X}}}{C_\sigma} = 1, \frac{C_\varepsilon \cdot C_E}{C_\sigma} = 1, C_V = 1. \quad (3)$$

Here,  $C_\sigma$  is the stress similarity ratio;  $C_u$  is the displacement similarity ratio;  $C_E$  is the elastic modulus similarity ratio;  $C_l$  is the geometric similarity ratio;  $C_v$  is the Poisson's similarity ratio;  $C_\varepsilon$  is the strain similarity ratio;  $C_{\bar{X}}$  is the surface force similarity ratio.

The shaft wall structure studied herein is a composite structure composed of reinforced steel, concrete, PVA fiber, and PPTF fiber. To ensure that the shaft wall model is strictly similar to the engineering prototype strain during the entire loading process,  $C_\varepsilon = 1$  is required. To ensure that the failure mode of the shaft wall model is similar to that of the prototype, the building materials of the model specimen were made the same as that of the prototype.

**Table 9** Design parameters of prototype shaft wall structure.

Inner diameter/m	Outer diameter/m	Wall thickness/m	Strength grade of concrete	Thickness-to-radial dimension ratio
10	12	1.0	HFRC70	0.2

Therefore, the similarity criterion of the shaft wall strength model test can be deduced as follows:

$$C_E = C_f = 1, C_\rho = 1, C_\xi = 1. \tag{4}$$

$$C_{\bar{X}} = C_\sigma = 1, C_u = C_l. \tag{5}$$

Here,  $C_\rho$  is the similarity constant of the steel ratio;  $C_\xi$  is the similarity constant of the mixed fiber ratio;  $C_f$  is the material strength similarity ratio.

Under these conditions, as long as the appropriate geometric similarity constant is determined, the real stress of the original shaft wall can be deduced from the model test results.

#### 4.1.2 Design of Model Parameter

To compare the results of the model test with the numerical simulation results and then verify the rationality of the numerical simulation method, the uneven load test of the shaft wall structure is based on the numerical calculation M-8 as the prototype in this model test. The hybrid-fiber-reinforced concrete configured above was used as the shaft wall building material. Table 9 presents the structural parameters of the prototype shaft wall in engineering.

Based on the deduced similarity index and design parameters of the prototype shaft wall structure and combined with the size of the laboratory loading device, the geometric similarity ratio was set to 4. Table 10 presents the design parameters of this model test.

#### 4.1.3 Model Preparation and Test Component Placement

The steps followed to prepare the model specimens of the shaft wall were as follows. First, the mold was processed



**Fig. 7** Layout of reinforcement cage.



**Fig. 8** Casted shaft wall model.

in a laboratory, and a reinforcement cage was prepared. The strain gauges were pasted in the four directions of the processed reinforcement cage, namely east, south, west, and north. Subsequently, the reinforcement cage was placed in the assembled mold, and a hybrid-fiber-reinforced concrete was poured. After pouring and curing the specimen for 3 days, the mold was removed, and the specimen was sprayed for curing. After 21 days, the surface of the model specimen was ground flat, and the strain gauge was pasted. Finally, the loading cylinder was arranged; Figs. 7 and 8 show the preparation process of the model.

**Table 10** Design parameters of model shaft wall structure.

Outer diameter/m	Inner diameter/m	Wall thickness/m	Thickness-to-radial dimension ratio
3.0	0.25	2.5	0.2
Model height /m	Strength grade of concrete	Polyvinyl alcohol fiber dosage /kg m <sup>-3</sup>	Polypropylene-imitated steel fiber content/kg m <sup>-3</sup>
0.21	HFRC70	1.092	5



**Fig. 9** Strain gauges installed on the steel cage.



**Fig. 11** Wellbore model test system.



**Fig. 10** Strain gauges installed on the concrete at the inner edge of the shaft wall.

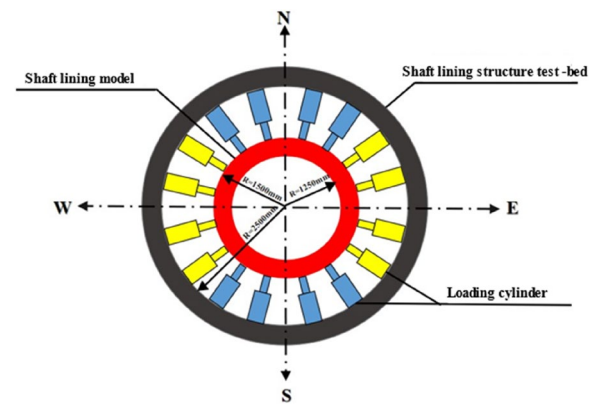


**Fig. 12** Schematic of model test loading.

To obtain the deformation and stress characteristics of the shaft wall model under the action of uneven loading, test elements should be arranged on the surface of the reinforcement and concrete specimens. The specific arrangement is as follows.

For the strain test of the shaft wall, four measuring points were arranged along four directions on the inner and outer steel meshes and the concrete surface on the inner edge of the shaft wall. The polishing process was first conducted, and a strain gauge was pasted in the vertical and annular directions of each measuring point, as shown in Figs. 9 and 10.

For the displacement monitoring of the shaft wall, to obtain the radial displacement of the shaft wall model during the loading process, four resistive displacement sensors were symmetrically arranged on the inner edge of the shaft wall model. Fig. 11 shows the entire model test system.

#### 4.2 Experimental Loading

In this model test, 16 hydraulic cylinders were used to apply an uneven load. At the same time, foundation bolts

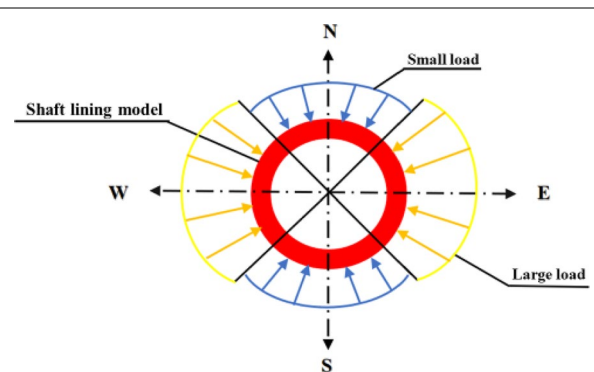


**Fig. 13** Load distribution of the shaft wall model structure.

and tie rods with sufficient stiffness were used for the vertical restraint to prevent the specimen from unstable deformation along the vertical direction. The entire model specimen was in the plane stress state, as shown in Fig. 12.

In the previous numerical simulation calculation, the uneven load is distributed in the form of a sine function; however, in the model test, this type of load distribution

is difficult to implement. Therefore, based on the test loading conditions, the load form shown in Fig. 13 is used for loading. Through a force analysis and equivalent principle, it can be seen that this loading mode is more unfavorable to the shaft wall structure than the sinusoidal distribution of the uneven load. The calculation results show that the coefficient of the uneven pressure applied by the test is 0.2, which is equivalent to 0.223 in the form of the sine function distribution (Yao & Sun, 1995).

Before the test loading, a preloading was conducted to check whether the loading system and test system operated normally. The pressure of the preloading cylinder was controlled at 3 MPa. Formal loading was then applied through the loading control system to set the target load to load step by step. Four pairs of oil cylinders were set in the east–west direction and four pairs in the north–south direction to apply two sets of load values, namely high and low loads. In this test, a high-load  $P_1$  is symmetrically applied to the east–west cylinder, and a low-load  $P_2$  is symmetrically applied to the south–north cylinder. The high and low loads were applied step by step synchronously. The entire loading process is as follows:

- (1) When the nonuniformity coefficient is 0.1, a high-load  $P_1$  is applied to the four oil cylinders in the east–west direction, and a low load  $P_2$  is applied to the four oil cylinders in the north–south direction, where  $P_1/P_2=1.1$ .
- (2) When the nonuniform coefficient is 0.2,  $P_1/P_2=1.2$ , and the load continues until the specimen is destroyed, the ultimate bearing capacity of the shaft wall model when the nonuniform load coefficient is 0.2 is obtained.

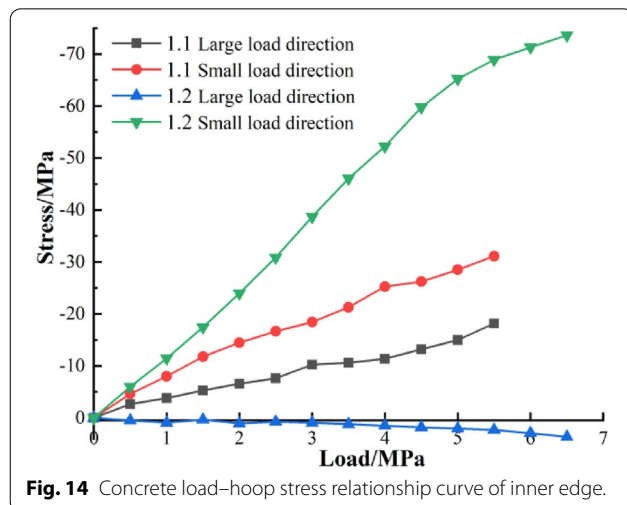


Fig. 14 Concrete load–hoop stress relationship curve of inner edge.

### 4.3 Test Results and Analysis

#### 4.3.1 Analysis of Shaft Wall Stress

The data collection system was used to collect data recorded by the strain gauge on the surface of the reinforcement and the concrete on the inner edge of the shaft wall model. The strain value under each load level was converted into the stress value (Yao et al., 2007, 2017), and the relationship between the model load and circumferential stress was plotted in the form of a curve, as shown in Figs. 14, 15, 16. The test curve was divided along the high- and low-load directions.

The load–circumferential stress curves in Figs. 14, 15, 16 show that the circumferential stresses of the concrete and steel bar in the shaft wall structure are positively correlated with the load. At the initial stage of loading, they are in an elastic stress state and reach their yield strength

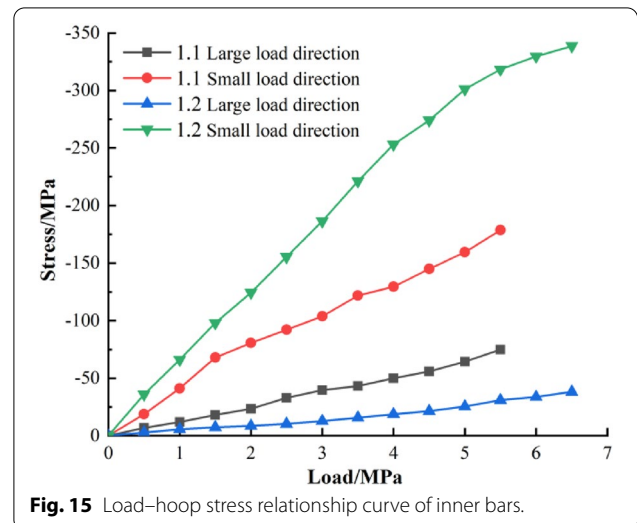


Fig. 15 Load–hoop stress relationship curve of inner bars.

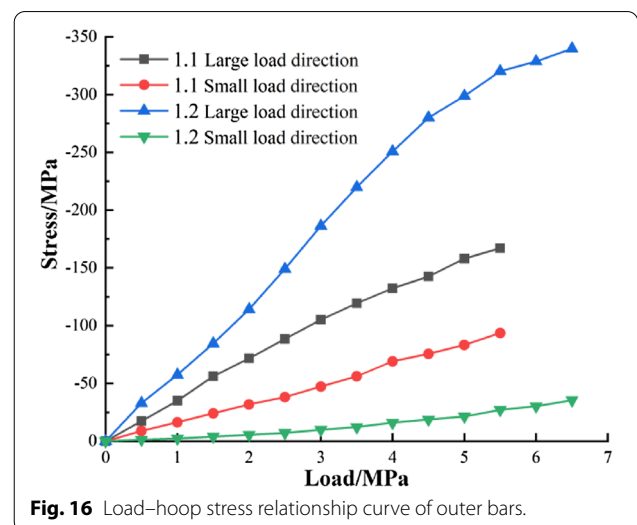


Fig. 16 Load–hoop stress relationship curve of outer bars.

as the load increases step by step. Moreover, in the high-load direction, the circumferential stress of the shaft wall presents a distribution law characterized by high values outside and low values inside. In the low-load direction, the distribution rule is high values inside and low values outside. When the nonuniformity coefficient is 1.1, the concrete and steel bars of the shaft wall are both under compressive stress, indicating that they are in a compression state. However, when the nonuniform coefficient is 1.2, the tensile stress appears in the direction of high load on the inner edge of the shaft wall, and the tensile stress reaches 3.8 MPa when the specimen is destroyed. However, the stress acting on the ordinary reinforced concrete shaft wall structure is unfavorable, leading to premature cracking of the concrete, thus reducing the bearing capacity of the shaft wall. Therefore, in this study, the hybrid-fiber-reinforced concrete was used instead of ordinary concrete as the shaft wall material, and the tensile strength of the material itself could be significantly improved, thus avoiding premature cracking of the concrete, so as to significantly improve the bearing capacity of the shaft wall under the action of uneven loads.

**4.3.2 Analysis of Shaft Wall Displacement**

The load–radial displacement curve of the shaft wall in the loading process is sorted and drawn, as shown in Fig. 17, where the negative ordinate value represents the inward displacement deformation of the shaft wall, and the positive value represents its outward displacement deformation.

Fig. 17 shows that under the action of uneven load, there are significant differences in the displacement and deformation of the shaft wall along the different directions. In the high-load direction, the shaft wall is displaced and deformed inward, while in the low-load

direction, the shaft wall displaces outward. The displacement due to inward contraction is slightly larger than that due to outward expansion. With the increase in the nonuniformity coefficient, this phenomenon is more evident, the radial displacement due to contraction and expansion in the high- and low-load directions is also larger. The relative displacement along the two directions easily causes bending failure of the shaft wall section, and the concrete is more prone to exhibit tensile stress. Therefore, using a hybrid-fiber-reinforced concrete material can significantly improve the ability of the shaft wall to bear uneven loads.

**4.3.3 Analysis of the Failure Form and Bearing Capacity of the Shaft Wall**

In the loading process under a nonuniform load coefficient of 1.2, with the increase in the load, the cracking sound of concrete could be heard, accompanied by the falling off of surface concrete. With further increase in the load, cracks appeared and gradually expanded in the shaft wall; however, there were no brittle characteristics, such as sudden fracture failure. The failure part of the specimen was the south inner edge of the shaft wall, that is, the inner edge in the low-load direction. This section of concrete was subjected to eccentric load and bending moment during loading, resulting in tensile stress, local cracks, and finally failure. Large cracks appeared in the model specimen at the failure location, and the failure surface was at an angle of approximately 40° with the circumferential tangent plane, presenting the characteristics of pull-shear failure, as shown in Fig. 18. From the cracks, it can be seen that the PPTF fibers were still connected on both sides of the failure surface, indicating that the hybrid fibers could significantly improve the ductility of the shaft wall structure, improve the failure characteristics of the shaft wall, and improve the degree of safety.

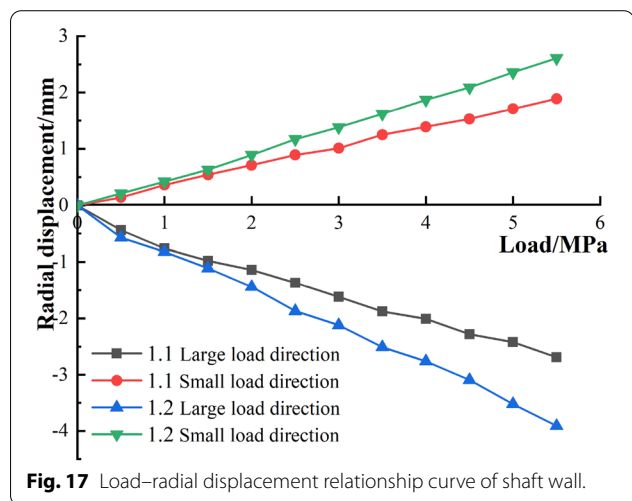


Fig. 17 Load–radial displacement relationship curve of shaft wall.



Fig. 18 Shaft wall failure state.

Through the loading test, the failure load of the shaft wall model was found to be 6.8 MPa under the low load and 8.2 MPa under the high load, which is the ultimate bearing capacity of the shaft wall. The relevant parameters of the shaft wall specimen (the compressive strength of the cube block with the hybrid-fiber-reinforced concrete in the shaft wall was 78.7 MPa in the test) were substituted into the regression formula (2) for the numerical simulation calculation of the ultimate bearing capacity, and the calculated low and high loads were 7.17 and 8.77 MPa, respectively. These values are relatively consistent with the test results, confirming the reliability of the numerical simulation results.

#### 4.4 Discussion

In this study, the mechanical properties of a hybrid-fiber-reinforced concrete shaft lining structure under uneven load were studied through numerical simulation and model tests. The research results showed that the error between the numerical simulation results and the model test results is approximately 5%. To place the study results in the context of existing literature, the results were compared with those obtained by Peng (2022) for the bearing capacity of C80–C90 high-strength reinforced concrete shaft lining structure. When the nonuniformity coefficient is 1.15, the circumferential compressive stress of the concrete at the inner edge of the shaft wall increases with the increase in the lateral pressure, the peak compressive stress is 36.63 MPa, the vertical stress is tensile, and the peak stress is 10.35 MPa. The stress at the inner and outer sides of the reinforcement increases with the increase in the lateral pressure. When the lateral pressure increases to 8.83 MPa, the peak compressive stress of the reinforcement reaches 243.14 MPa, and the average displacement at the inner side of the shaft wall shows a linear growth trend. This is consistent with the results of this study. However, due to the significant difference in the selection of model materials between the two studies, there is a significant difference in the numerical values; therefore, the test results cannot be considered consistent.

## 5 Conclusions

- (1) Based on the physical mechanism of the shaft wall in deep rock stratum and the outer shaft wall of a frozen shaft in a deep loose layer, to prevent shaft wall structures made of concrete from undergoing tensile failure under the action of an uneven load, this study adopted hybrid-fiber-reinforced concrete as the construction material for the shaft wall. Through an orthogonal test, the optimum mixture

ratio of the hybrid-fiber-reinforced concrete was determined.

- (2) Using ANSYS, a numerical analysis model of the shaft wall structure made of hybrid-fiber-reinforced concrete under uneven loading was established. The calculation results showed that the shaft wall structure exhibits tensile stress under the action of nonuniform load, and adopting hybrid-fiber-reinforced concrete instead of ordinary concrete as the wall building material could improve the resistance of the shaft wall structure to nonuniform loads.
- (3) Based on the data simulation results and using a range analysis method, the order of factors mainly affecting the bearing capacity of the structure under uneven loading was the thickness ratio of the shaft wall, concrete strength, and uneven pressure coefficient. From the numerical simulation results, the calculation formula for the shaft wall bearing capacity was obtained by regression.
- (4) The model test conducted on the hybrid-fiber-reinforced concrete shaft wall structure under the action of uneven loading showed that when the coefficient of the uneven load was 1.2, the tensile stress along the inner edge of concrete in the high-load direction was 3.8 MPa, which was unfavorable to the shaft wall. When loading failure occurred, the ultimate bearing capacity of the shaft wall was 6.8 MPa under low load and 8.2 MPa under high load, consistent with the calculation results of the numerical simulation regression formula, confirming the reliability of the numerical simulation results.
- (5) This study showed that the use of a hybrid-fiber-reinforced concrete as the shaft wall structure material can help significantly improve its ability to resist uneven loads, improve the brittle failure characteristics of concrete, and improve its reliability. It represents an excellent material for deep shaft wall structures.

#### Authors' information

Zhishu Yao is a professor and doctoral supervisor of the school of civil architecture, Anhui University of Science and Technology, Huainan, Anhui, 232001, China.

Yongjie Xu is a doctoral student of the school of civil architecture, Anhui University of Science and Technology, Huainan, Anhui, 232001, China.

Ping Zhang is a graduate student of the school of civil architecture, Anhui University of Science and Technology, Huainan, Anhui, 232001, China.

Yu Fang is a doctoral student of the school of civil architecture, Anhui University of Science and Technology, Huainan, Anhui, 232001, China.

Chen Wang is a graduate student of the school of civil architecture, Anhui University of Science and Technology, Huainan, Anhui, 232001, China.

Naihao Diao is a graduate student of the school of civil architecture, Anhui University of Science and Technology, Huainan, Anhui, 232001, China.  
Kun Hu is a graduate student of the school of civil architecture, Anhui University of Science and Technology, Huainan, Anhui, 232001, China.

### Acknowledgements

The authors would like to acknowledge participation of Master team of College of Civil Engineering in the experimental works, and particularly appreciate the valuable comments made by the editors and reviewers to make a substantial improvement to this manuscript.

### Author contributions

ZY: review, formal analysis, supervision. YX: writing, investigation, formal analysis, software, validation. PZ: investigation, formal analysis, supervision. YF: sample acquisition, tools and equipment handing. CW: sample acquisition, conducted the experiments. ND: investigation, formal analysis, review. KH: data curation, supervision. All authors read and approved the final manuscript.

### Funding

This research was supported by the National Natural Science Foundation of China (Nos. 52174104 and 51674006) and Provincial Natural Science Foundation of Anhui (YJS20210410).

### Availability of data and materials

Some of all the data, models, or code that support the findings of this study are available from the corresponding author upon reasonable request.

### Declarations

#### Competing interests

The authors declare that they have no known competing financial interests or personal relationships that could have appeared to influence the work reported in this paper.

Received: 22 March 2022 Accepted: 28 June 2022

Published online: 17 October 2022

### References

- Cheng, H., Zhang, L. L., Yao, Z. S., Peng, S. L., & Guo, L. H. (2021). Mechanism of shaft deflection in asymmetric mining of thick unconsolidated layer and thin bedrock. *China Coal Soc.*, 46(01), 1283–1305. <https://doi.org/10.13225/j.cnki.jccs.2021.1510>
- China Coal Construction Association. (2016). *GB50384-2007, Code for design of coal mine shaft and chamber*. Beijing: China Planning Press.
- Cui, Y. L. (2003). *A concise handbook of mine construction engineering*. Beijing: China Coal Industry Press.
- Fang, Y., Yao, Z. S., Huang, X. W., Li, X. W., Diao, N. H., Hu, K., & Li, H. (2022). Permeability evolution characteristics and microanalysis of reactive powder concrete of drilling shaft lining under stress-seepage coupling. *Constr Build Mater*, 331, 127296. <https://doi.org/10.1016/j.conbuildmat.2022.127336>
- Gao, Y. L., He, Q. Y., Li, C. P., Wang, M., Han, X. L., Ma, B., et al. (2021). Analysis of shaft failure mechanism in the 1240–1120 m section of Xi'er auxiliary shaft in Longshou mine of Jinchuan deposit. *Sci Technol Eng*, 21(23), 64–67.
- Guler, S., & Yavuz, D. (2019). Post-cracking behavior of hybrid fiber-reinforced concrete-filled steel tube beams. *Constr Build Mater*, 205, 285–305. <https://doi.org/10.1016/j.conbuildmat.2019.01.192>
- Guler, S., Yavuz, D., & Aydin, M. (2019a). Hybrid fiber reinforced concrete-filled square stub columns under axial compression. *Eng Struct*, 198, 109504. <https://doi.org/10.1016/j.engstruct.2019.109504>
- Guler, S., Yavuz, D., Korkut, F., & Ashour, A. (2019b). Strength prediction models for steel, synthetic, and hybrid fiber reinforced concretes. *Struct Concr*, 20(1), 428–445. <https://doi.org/10.1002/suco.201800088>
- Han, T., Yang, W. H., Ren, Y. L., & Yang, Z. J. (2012). Numerical and experimental model studies of the horizontal bearing properties of shaft linings of encased steel or steel fiber reinforced, high strength concrete. *J China Univ Min Tech*, 41(02), 205–211.
- He, M. C. (2021). Research progress of deep shaft construction mechanics. *China Coal Soc*, 44(05), 1283–1305. <https://doi.org/10.13225/j.cnki.jccs.YT21.0124>
- Hsie, M., Tu, C. J., & Song, P. S. (2008). Mechanical properties of polypropylene hybrid fiber-reinforced concrete. *Mater Sci Eng A*, 494, 153–157. <https://doi.org/10.1016/j.msea.2008.05.037>
- Jiang, G. J., Wang, J. P., & Liu, X. M. (2013). Study on frozen pressure measurement of ultra thick clay stratum. *Coal Sci Tech*, 41(03), 43–46. <https://doi.org/10.13199/j.cst.2013.03.49.jianggj.017>
- Kong, W. H., Yang, L., Yao, Z. S., Xue, W. P., & Gao, C. (2020). Preparation and crack resistance test of high performance concrete with fiber hybrid and micro expansion freezing shaft wall. *Saf Coal Mines*, 35(03), 45–48. <https://doi.org/10.13347/j.cnki.mkaq.2020.03.014>
- Liang, N. H., Ren, L. X., Tian, S., Liu, X. R., Zhong, Z. L., Deng, Z. Y., & Yan, R. (2021). Study on the fracture toughness of polypropylene-basalt fiber-reinforced concrete. *Int J Concr Struct Mater*. <https://doi.org/10.1186/s40069-021-00472-x>
- Liu, Z. Q., Song, C. Y., Ji, H. G., Liu, S. J., Tan, J., Cheng, S. Y., & Ning, F. B. (2021). Construction mode and key technology of mining shaft engineering for deep mineral resources. *China Coal Soc*, 46(03), 1283–1305. <https://doi.org/10.13225/j.cnki.jccs.yt20.1944>
- Naser, M. Z., & Hawileh, R. A. (2018). Predicting the response of continuous RC deep beams under varying levels of differential settlement. *Front Struct Civil Eng*, 13, 686–700. <https://doi.org/10.1007/s11709-018-0506-2>
- Peng, F. (2022). Research on bearing capacity of C80–C90 high strength reinforced concrete shaft lining structure. *China Coal Res Inst*. <https://doi.org/10.1007/s11709-018-0506-2>
- Qin, B. D., Liu, X. L., & Liu, S. F. (2017). Experimental study on ultimate strength and failure characteristics of hybrid fiber high strength concrete shaft wall. *Railw Eng*, 2017(01), 156–159.
- Shi, F., Pham, T. M., Hao, H., & Hao, Y. F. (2020). Post-cracking behaviour of basalt and macro polypropylene hybrid fibre reinforced concrete with different compressive strengths. *Constr Build Mater*. <https://doi.org/10.1016/j.conbuildmat.2020.120108>
- Shu, E., Song, H. Q., Cai, H. B., & Hong, R. B. (2021). Analysis on heterogeneity of freezing pressure in deep mine shafts of coal mine. *Mine Constr Tech*, 42(4), 45–51. <https://doi.org/10.19458/j.cnki.cn11-2456/td.2021.04.009>
- Sun, S. Y., & Yao, Z. S. (2017). Design and application of mixture ratio of high strength and high performance concrete for frozen shaft wall. *Mine Constr Technol*, 38(01), 1–4. <https://doi.org/10.19458/j.cnki.cn11-2456/td.2017.01.001>
- Wang, J. Z., & Qi, S. Z. (2005). Application of high strength concrete in deep soil shaft wall. *Mine Constr Technol*, 2005(06), 32–35. <https://doi.org/10.19458/j.cnki.cn11-2456/td.2005.06.010>
- Yang, J. J. (2005). *Similitude theory and structural model test*. Wuhan: Wuhan University of Technology Press.
- Yang, H. R., & Li, M. J. (2016). Fracture mechanism analysis and treatment measures of outer shaft wall during construction period by freezing method. *Coal Technol*, 35(3), 68–70. <https://doi.org/10.13301/j.cnki.ct.2016.03.027>
- Yang, L., Yao, Z. S., Xue, W. P., Wang, X. S., Kong, W. H., & Wu, T. L. (2019). Preparation, performance test and microanalysis of hybrid fibers and micro expansive high-performance shaft wall concrete. *Constr Build Mater*, 223(2019), 431–440. <https://doi.org/10.1016/j.conbuildmat.2019.06.230>
- Yao, Z. S., & Sun, W. R. (1995). Experimental study on concrete lining structure of frozen shaft under uneven lateral pressure. *J Fuxin Min*, 1995(03), 30–33.
- Yao, Z. S., Cheng, H., & Rong, C. H. (2007). Research on stress and strength of high strength reinforced concrete drilling shaft wall in thick top soils. *J China Univ Min Technol*, 2007(03), 432–435. [https://doi.org/10.1016/S1006-1266\(07\)60120-5](https://doi.org/10.1016/S1006-1266(07)60120-5)
- Yao, Z. S., Song, H. Q., & Cheng, H. (2009). Development of high performance concrete for frozen shaft wall and experimental study on its main mechanical properties. *Coal Eng*, 2009(12), 36–39.
- Yao, Z. S., Cheng, H., Ju, X. B., & Jiang, K. Y. (2015). Measurement and analysis of freezing pressure in deep clay stratum. *Mine Constr Technol*, 36(04), 30–33. <https://doi.org/10.19458/j.cnki.cn11-2456/td.2015.04.014>
- Yao, Y. F., Cheng, H., Li, M. J., Rong, C. X., & Song, J. (2016). Fuzzy random finite element reliability and sensitivity analysis of reinforced concrete outer shaft lining structure in deep alluvium. *J China Coal Soc*, 41(12), 3032–3039. <https://doi.org/10.13225/j.cnki.jccs.2016.0547>
- Yao, Z. S., Cheng, H., & Ju, X. B. (2017). Research and application of high strength steel-fiber concrete compound shaft wall with inner steel plate in deep

- alluvium shaft repair. *China Coal Soc*, 276, 2295–2301. <https://doi.org/10.13225/j.cnki.jccs.2016.1790>
- Yao, Z. S., Li, X., Wu, T. L., Yang, L., & Liu, X. H. (2019). Hybrid-fiber-reinforced concrete used in frozen shaft wall structure in coal mines. *Materials*, 12(23), 3988. <https://doi.org/10.3390/ma12233988>
- Yao, Z. S., Wang, C., Xue, W. P., Zhang, P., & Fang, Y. (2021). Experimental study on the dynamic mechanical properties of high-performance hybrid fiber-reinforced concrete of mine shaft wall. *J Mater Res Technol*, 2021(14), 888–900. <https://doi.org/10.1016/j.jmrt.2021.07.015>
- Zhang, J. J., Zhang, X. D., & Wu, Z. J. (2014). Research on mechanical behavior of concrete shaft wall under non-uniform lateral pressure. *J Guangxi Univ*, 39(02), 237–244. <https://doi.org/10.13624/j.cnki.issn.1001-7445.2014.02.006>
- Zhang, W., Wang, B. S., & Wang, Y. (2018). Elastic analysis of nonhomogeneous frozen wall under nonaxisymmetric ground stress field and in state of unloading. *Adv Mater Sci Eng*, 2018(5), 1–13. <https://doi.org/10.1155/2018/2391431>
- Zhang, P., Yao, Z. S., Xue, W. P., & Mu, K. H. (2020). Study on mechanical properties and microstructure of hybrid fiber shaft wall concrete. *J Anhui Univ Sci Technol*, 40(03), 33–38.
- Zhao, J., & Lin, B. (2014). Stress measurement analysis of freezing shaft wall in Gubei mine auxiliary shaft. *Coal Mine Saf*, 45(05), 183–186.

### Publisher's Note

Springer Nature remains neutral with regard to jurisdictional claims in published maps and institutional affiliations.

Submit your manuscript to a SpringerOpen<sup>®</sup> journal and benefit from:

- Convenient online submission
- Rigorous peer review
- Open access: articles freely available online
- High visibility within the field
- Retaining the copyright to your article

---

Submit your next manuscript at ► [springeropen.com](https://www.springeropen.com)

---